HHS Public Access

Author manuscript

Addit Manuf. Author manuscript; available in PMC 2021 January 01.

Published in final edited form as:

Addit Manuf. 2020 January ; 31: . doi:10.1016/j.addma.2019.100931.

Functional Bimetallic Joints of Ti6Al4V to SS410

Bonny Onuike, **Amit Bandyopadhyay***

W. M. Keck Biomedical Materials Research Lab, School of Mechanical and Materials Engineering, Washington State University, Pullman, WA 99164-2920, USA.

Abstract

Bimetallic structures provide a unique solution to achieve site-specific functionalities and enhanced-property capabilities in engineering structures but suffer from bonding compatibility issues. Materials such as titanium alloy (Ti6Al4V) and stainless steel (SS410) have distinct attractive properties but are impossible to reliably weld together using traditional processes. To this end, a laser-based directed energy deposition (DED) system was used to fabricate bimetallic joint of Ti6Al4V and SS410 keeping niobium (Nb) as a diffusion barrier layer. Both shear and compression tests were used to characterize the joint's strength, and compared with the base materials. The bimetallic-joint shear and compressive yield strengths were 419± 3 MPa (~ 114 % of SS410) and 560 ± 4 MPa (~ 169 % of SS410), respectively. The increase in interfacial shear and compressive yield strengths over the base material indicates strong metallurgical bonding between the base materials and the interlayer, Nb. Proof-of-concept part for direct application of the bimetallic joint was demonstrated by welding base metals, end-to-end, to the joint. The interfacial microstructures, elemental diffusion and phases, including failure modes were examined using secondary and backscatter electron imaging, X-ray diffraction (XRD) and energy dispersive spectroscopy (EDS). The bimetallic-joint interfaces were free from brittle intermetallic compounds such as FeTi and Fe_2Ti that are generally responsible for weak bond strength.

Graphical Abstract

* amitband@wsu.edu.

Conflict of interest: None

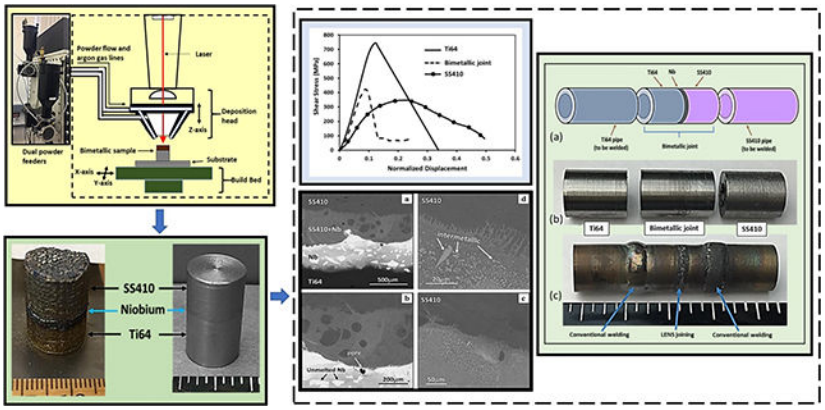

Keywords

Directed energy deposition; Bimetallic joint; Ti6Al4V; SS410; Mechanical properties

1. Introduction

The need for enhanced properties and site-specific functionality of engineering materials for advanced applications has spurred the development of multi-materials structures [1, 2]. Materials such as titanium alloy and stainless steel have attractive properties with extensive applications in aerospace, petroleum/petrochemical processing, and biomedical industries. For example, Ti6Al4V (Ti64), the most common titanium alloy, offer excellent corrosion and fatigue resistance characteristics, including high strength to weight ratio. This material is used in aerospace engine compressor blades [3] and load-bearing implants [4, 5]. Martensitic stainless-steel type 410 (SS410), on the other hand, exhibits good corrosion resistance, ductility and tensile strength along with magnetic properties. SS410 is widely used in power-plant and gas turbines including petroleum fractionating components [6, 7]. To benefit simultaneously, from the exclusive properties of the two alloys in a single overall structure, the development of a Ti64/SS410 bimetallic joint is necessary.

Several manufacturing techniques have been devised to develop bimetallic joints of titanium or its alloy with stainless steel. Conventional method involves fusion of the base materials via different bonding strategies. Direct bonding of commercially pure titanium (CPTi) or Ti64 with different types of stainless steels have been attempted through laser and explosive welding [8–10] methods including friction stir welding [11, 12]. Transient liquid phase process [13, 14] and diffusion bonding [15–18] have also been used. With the development of directed-energy-deposition (DED) based additive manufacturing (AM) method, bimetallic joints can be manufactured in a single-step with added functionalities. Both direct deposition and compositional gradation of Ti64 with various stainless steels, such as SS304 and SS316 [19, 20], have been attempted using AM method. However, irrespective of the manufacturing technique used, the inherent issues associated with dissimilar metals bonding, like interfacial cracking and delamination caused by mismatch in thermal properties were observed. Chen et al. [9] had reported weld cracks during direct laser welding of CPTi to SS304. During direct bonding, wide variation in coefficient of thermal expansion (CTE) between the base metals

induce thermal/residual stresses. These stresses promote crack initiation / propagation at the interface leading to weak strength or failure of the joints.

Apart from interfacial cracking, debonding features caused by formation of brittle intermetallic phases at the interfacial region due to mismatch in metallurgical properties is another challenge. The mechanism leading to formation of such phases is attributed to limited solubility of one element into another. This is specifically seen in the phase diagram of the dissimilar materials' main component elements. For example, in Ti-alloy and stainless steel bimetallic joint, the main constituent elements of the base-alloys are Ti and Fe. Both elements form brittle intermetallic phases of FeTi and Fe_2Ti due to limited solubility of Fe in Ti, which occurs at about 51 to 54 wt% and 68 to 75 wt % of Fe [21]. Formation of these brittle intermetallic phases were previously reported during diffusion bonding of CPTi/Ti64 with SS304 [13, 16] and LENS™ processing of Ti64-SS316 bimetallic joint [20]. Practically, if dissimilar metals fail during direct bonding, then, compositional gradation is also difficult. Such was evident during an attempt to bond Ti64 with SS304, SS316 and Inconel 718 [19, 20, 22].

In an attempt to mitigate the challenges associated with dissimilar metal bonding through direct joining or compositional gradation, an intermediate-bond-layer (IBL) build strategy was conceptualized. The IBL is a third material that acts as a bond-link and diffusion barrier to the immiscible elements of the dissimilar metals. In practice, it's essential to select an appropriate bond material which will improve the bimetallic joint's interfacial bond strength via attenuating brittle intermetallic phase formation, including lowering the interfacial residual and thermal stresses that induce/propagate cracks. Many researchers have used various IBLs ranging from single materials like Nickel (Ni) [23, 24], Copper (Cu) [25 – 27], Silver (Ag) [28] and Niobium (Nb) [29] to multi-material-alloy interlayers such as Ag-Cu [30], NiCr [20] and Nb/Cu/Ni [31, 32] to bond Ti/Ti-alloys with various stainless steels. Similar issues observed during composition gradation including low bond strength compared to the base material were reported almost in all cases. For example, Kundu et al. [23, 24] and Sahasrabudhe et al. [20] reported brittle intermetallic phases of Ni_3Ti, NiTi and Ni_2Ti, alongside de-bonding features during diffusion bonding of CPTi to SS304 with Ni interlayer and LENS processing of Ti64/SS316 bimetallic joint with NiCr interlayer. Likewise, the interfacial bond strength obtained from diffusion bonded CPTi/stainless steel joint with copper interlayer was about 38% compared to SS304 [25]. The reason for such low bond strength was either due to inappropriate method of joining employed or use of incompatible interlayer for the base materials.

In this study, a laser DED-based additive manufacturing (AM) method, was used to fabricate Ti64/SS410 bimetallic joint with Nb interlayer. Meanwhile, niobium is a β-stabilizer to Ti, and forms ε-Fe_2Nb stable phase. Among AM process, laser engineered net shaping (LENS™) system can manufacture complex multi-materials structures with added functionality in a single-step operation. Bimetallic joints produced via LENS are more likely to be stronger in comparison to other joining techniques because metallurgical bonding of materials at the interface is greatly enhanced due to improved diffusion of elemental compositions and refined microstructure during laser processing [33]. The Ti64/SS410 bimetallic joint's interfacial shear strength including the overall structure's compressive

yield strength were evaluated and results compared with the parent materials. The development of such advanced composite material joint will potentially enhance the weldability of dissimilar materials via end-to-end to the bimetallic joint. Also, the bimetallic structure will improve system performance for various applications, like stator-rotor assembly of power generation system which may require high strength-to-weight ratio at the outer-section and ferromagnetic property at the inner-section.

2. Materials and methods

For the LENS™ processing of Ti64/SS410 bimetallic joint, Ti64, SS410 and Nb powders were procured from Hoeganaes Corporation (Cinnaminson, NJ, USA), Höganäs (Belgium S.A.) and H. C. Starck (MA, USA), respectively. All powders were sieved to particle size range: −150 μm/+45 μm. Also, Ti64 and SS410 build plates of dimensions 15 cm X 10 cm X 0.32 cm thick were used. The SS410 chemical composition by wt % are 85Fe, 11.5 to 13.5Cr, < 0.15C, > 0.75Ni, including trace of Mn, Si, P and S. Ti64 contains by wt %: 90Ti, 6Al and 4V.

2.1. LENS™ processing of the bimetallic joint

Laser engineered net shaping (LENS™) is a directed energy deposition-based AM system with multi-functional capabilities such as multi-powder feeders. This feature permits simultaneous deposition of different materials without stopping the machine for powder change, and enhances efficient manufacturing of multi-material structures in a single-build operation. For this reason, LENS™ system was used to manufacture Ti64/SS410 bimetallic joint with Nb as interlayer. During deposition, the LENS compartment is circulated with argon (Ar) to keep O_2 level below 10 ppm to limit oxidation of the build part. The powder feeders, deliver Ti64, Nb and SS410 powders, via argon gas transport, into the melt pool generated by Nd -YAG laser beam. Deposition process transitioned from Ti64→Nb→SS410. That's, Ti64 material of about 14mm diameter and 8mm height was initially deposited on its substrate followed by deposition of 3 layers of Nb, about 300μm thick, on top of the Ti64. Subsequently, SS410 was deposited on the Nb layer and the overall height of Ti64/SS410 bimetallic structure formed about 15mm, as shown in Fig. 1a. Pure samples of Ti64 and SS410 were also built, and Table 1 shows the LENS processing parameters for the entire build.

2.2. Interfacial joint characterization

After printing the Ti64/SS410 bimetallic structures and the base materials samples, selected bimetallic joint samples were sectioned perpendicular to the interface using water-jet cutter. The cross-section surface was wet-ground and polished using silicon carbide (SiC) grinding paper and alumina-DI water suspension (from 0.1μm to 0.05μm), respectively. Interfacial microstructure was examined using backscatter secondary electron (BSE) detector. Phase II Micro Vickers Hardness Tester (Model 900–391) was used to measure microhardness across the interface at 1.98 N load (HV0.2), keeping hold time at 15s. Elemental compositions within the interfacial region was mapped using Energy Dispersive Spectroscopy (EDS) analysis. X-ray diffraction (XRD) (Rigaku Smart Lab diffractometer) analysis with Cu Kα

radiation was conducted across the bimetallic interface for phase identification at a 2θ range from 20 to 90 degrees keeping step size at 1 degree per minute.

2.3. Bond strength measurement

The LENS™ processed bimetallic joints, including the pure Ti64 and SS410 samples were cut to 3mm diameter by 11mm length using water-jet machine for shear test. Single-shear test device [34], developed in our lab, was used to characterize the shear strength of these samples. The interfacial bond-line of the bimetallic structure was accurately positioned on the shear device centerline according to the test procedure described in reference 34 [34]. Likewise, 3mm square base by 6mm height specimens were cut, as well, for compression test and Shimadzu compression testing machine (AG-15, Kyoto, Japan) was used to perform the test at a feed rate 0.33 mm/min. Scanning electron microscopy (SEM) (FEI-SIRION, Portland, OR) at 20 kV (3.0 spot size and working distance of 9 mm) and BSE imaging were done to examine the fractography of the sheared surfaces and the cross-sections of the deformed samples, respectively.

3. Results

Successful manufacture of Ti64/SS410 bimetallic joint with Nb interlayer via LENS process was demonstrated. Both as-printed and machined samples are shown in Fig. 1a and b, respectively. Interfacial features/properties like microstructure, microhardness and bond strength were examined and mechanical reliability evaluated. The bimetallic interfacial shear strength, including the overall structure's compressive yield strength were measured and compared to the base-materials. One of the direct applications of the bimetallic joint is presented in Fig. 2a. Machined tubes of the base metals, Figs. 1c and 2b, were welded to the respective ends of the LENS processed bimetallic joint to demonstrate a proof-of-concept part, as shown in Fig. 2c. The welded assembly shows the viability of the LENS processed bimetallic-joint for dissimilar metals joining, which were almost impossible to join directly using conventional methods.

3.1. Interfacial microstructure and hardness profile

Fig. 3 shows the bimetallic-joint's interfacial microstructures. Un-melted particles of Nb are seen as white patches within the bond layer. A mixing zone containing stainless steel and niobium (SS410+Nb) can be seen as well in Fig. 3a and b. At high magnification in Fig. 3c and d, intermetallic phases including dendritic arms of most likely Fe-Nb phases were seen growing into the SS410 region, but with no cracks or de-bonding features. Similar diffusion zone and mixture phase have been reported elsewhere [29]. In Figs. 4a and b, EDS dot maps and line scan across the bimetallic interfacial-joint reveals upwards diffusion of elements such as Ti and V into Nb interlayer as well as diffusion of Nb into SS410 region. XRD analysis on the interfacial region, Fig. 5, shows different phases and diffraction peaks. The primary phases observed with the highest intensities are α-Ti (101), β-Ti (200), α-Fe (110) and Nb (222) identified at 40.2°, 44.6°, 44.7°, and 78.2°, respectively. The secondary phases/peaks, among others are NbC (111) and FeNb (306), identified at 35.3° and 69.1°, respectively. No brittle intermetallic phases like FeTi and Fe_2Ti can be found. Fig. 6 shows the hardness distribution over the bimetallic interface as a function of position. At the bulk

of Ti64 and Ti64/Nb interface, hardness values were 3.8 ± 0.8 GPa and 3.1 ± 0.21 GPa, respectively. It increased to 5.1 ± 0.38 GPa at the SS410/Nb interface and dropped to 1.6 ± 0.10 GPa at the bulk of SS410. The hardness trend within the interfacial zone was not surprising due to diffusion of elements and reaction products, including heat affected zone at the region.

3.2. Bimetallic structure bond strength

Fig. 7 shows the schematic of the shear device used for the shear strength test on the LENS processed Ti64, SS410 and the bimetallic-joint samples. Fig.8 shows the shear stress-normalized displacement curves and the shear strengths of the samples. Normalized displacement used in this context is simply the ratio of sample's displacement during shear to initial diameter. The shear deformations for Ti64 and the bimetallic-joint samples exhibited sharp failure points, as seen in Fig. 8a, a characteristic failure behavior of brittle material. Meanwhile, SS410 sample showed a failure pattern, typical of ductile material, with no distinct elastic/plastic transition point. This is expected, because SS410 material exhibits good ductile characteristics with large percent elongation. The shear strength of Ti64 sample was 740 ± 4 MPa, the bimetallic interfacial-joint was 419 ± 3 MPa and the lowest was SS410 with 367 ± 6 MPa. Here, the shear strength of the LENS processed Ti64 material was high in comparison to literature data, 550 MPa [35], in annealed condition. This could be attributed to improved microstructural characteristics during LENS processing. On the other hand, the shear strength of SS410 sample was comparable to 400 ± 17 MPa for commercial SS410 (annealed) that was tested.

SEM images in Fig. 9 show all sheared samples' surface morphologies. The Ti64 sample's fractography, Fig. 9a, reveals cleavage and flat islands with some shallow dimples. These features resemble a brittle fracture pattern. Similarly, Fig. 9c shows the fractography of SS410 with coarsen dimples and protrusions. These features resemble a fracture behavior of ductile material. In Fig. 9b, the bimetallic joint's fractography shows cleavage and intergranular fracture, which resembles, more likely, brittle failure mode as depicted in Fig. 8a.

The compressive stress-strain curves of all samples are shown in Fig. 10a. Here, Ti64 sample exhibited distinct elastic, alongside plastic deformation zones compared to SS410 and bimetallic-joint samples. Fig. 10b shows the 0.2% compressive yield strength (YS) of the samples. Ti64 YS was the highest with 1224 ± 34 MPa which is comparable to 1.15 GPa [36] (in wrought condition), while the bimetallic joint was 560 ± 4 MPa and the lowest was SS410 with 331± 21 MPa. The low YS of SS410 sample processed via LENS in comparison to literature, 551 MPa (tensile) [37] for cold rolled condition, could be attributed to presence of residual porosity that resulted into the density (6.7 ± 0.04 g/cm^3) compared to 7.8 g/cm^3 for commercial product. In Fig. 11, BSE images compare interfacial features of the bimetallic sample before and after compression test. Vertical cracks were observed at the SS410/Nb interface after deformation, but seemed arrested at the Nb region, Fig. 11b. The entire test results for shear and compression strengths are presented in Table 2.

4. Discussion

Researchers have employed different bonding processes, including use of IBL strategy to develop bimetallic joints of titanium and its alloys with stainless steels. One primary reason for these on-going efforts was to produce a mechanically reliable bimetallic joint and benefit, distinctly, from the unique properties of the two alloys. But, to achieve that goal, a combination of appropriate IBL and bonding process is essential. In our work, we have employed a unique approach to demonstrate a successful build of Ti64 and SS410 bimetallic joint using Nb interlayer. Mechanical reliability of the joint was evaluated with the base materials serving as controls. A concept-model part (Fig. 2a) designed for the direct application of the bimetallic joint illustrated how two immiscible dissimilar metals can be welded to various ends of the LENS processed bimetallic joint. A proof-of-concept part for such model was demonstrated, Fig. 2c, which shows the capability of our DED-based AM processed bimetallic joint, as a structural assembler for immiscible dissimilar materials. With this strategy, both short joints and long pipes/tubes of difficult-to-weld materials can be joined with ease.

4.1. Interfacial features

Among various challenges associated with bimetallic joint processing, selection of suitable etchant for metallographic study of the interfacial microstructure of composite materials is quite difficult. BSE imaging in SEM, which detect contrast on region based on z-value of the chemical compositions, was used to examine the interfacial-joint microstructures. In Fig. 3a and b, un-melted particles of Nb, seen as white patches, were evenly distributed within the bond region. Such incomplete melting could be attributed to the Nb's high melting point (2477°C) and insufficient energy density per unit volume, a function of laser power and other parameters, applied during Nb deposition on Ti64 surface.

While diffusion of Ti64 elements into the bond layer was not easily discernable in the BSE image (Fig. 3) due to low variation in contrast intensity, diffusion of Nb into the SS410 zone was apparent that resulted into a "mixing-zone". This zone is enriched with most likely FeNb phase, alongside intermetallic phases. Such reaction products are not uncommon. Kundu et al., [29] had reported similar phases like Fe_2Nb and Fe_7Nb_6 on diffusion bonded Ti/SS304 bimetallic joint with Nb-interlayer. Dendritic arms of FeNb phase, including intermetallics, preferentially grew into the SS410 region, Fig. 3c and d, towards the heat source as temperature gradient varies along the build part. However, the interfacial region was free of cracks or de-bonding features, an indicative of good metallurgical bonding resulting from the compatibility of Nb material to Ti64 and SS410. This is expected since Nb is a beta (β) stabilizer and also forms β-Ti+Nb and ε-Fe_2Nb stable phases. From the EDS dot map and line scan in Figs. 4a and b, diffusion of both Ti and V elements into Nb bond-layer, as well as diffusion of Nb into SS410 region can be seen to promote the formation of β-Ti+Nb and FeNb alongside other phases. Both primary and secondary phases, including NbC and Cr_5Al_8, intermetallics, were identified in the XRD diffraction peaks in Fig. 5. But, no brittle intermetallic phases of Fe-Ti, like FeTi and Fe_2Ti, were identified. Presence of these Fe-Ti phases are detrimental to the bimetallic-joint's strength, and negatively influences the mechanical reliability of the bimetallic structure. Therefore,

Nb acted not only as an IBL, but more importantly, as a diffusion barrier layer mitigating the formation of such brittle intermetallic phases.

Hardness distribution across the bond region can significantly influence the mechanical reliability of the bimetallic joint. At Ti64/Nb interface, hardness value was slightly low in comparison to 3.8 ± 0.8 GPa observed at the bulk of Ti64, Fig. 6. This could be due to small heat affected zone during initial deposition of Nb at high power setting. Similarly, the increase in hardness to about 5 GPa observed at the SS410/Nb interface could be attributed to the formation of intermetallic phase like NbC. Kundu et al. [29] and Vigraman et al. [13] had reported an increase in hardness during diffusion bonding of CPTi to SS304 with Nb interlayer, and Ti64 to SS304, respectively. The average hardness value recorded at Nb/SS304 and Ti64/SS304 interfaces was about 8.3 GPa [29, 13], ascribed to high concentration of intermetallic phases at the region. However, with LENS processing, interfacial elemental diffusion is greatly improved, including refined microstructures, which lowers such property mismatches as was observed in our case.

4.2. Bond strength analysis

High-dependability on bimetallic structures to meet on-demand or site-specific functionalities requires a joint with high interfacial strength comparable to the base materials. In principle, interfacial bond strength provides, among others, a performance measure to access the mechanical reliability of the structure. From our study, the bimetallic-joint and Ti64 samples showed similar shear deformation behaviors with distinct elastic zone and sharp failure points that resembles embrittled materials. However, SS410 samples behaved differently with large percent elongation, typical for a ductile material, Fig. 8a. For the bimetallic-joint's interface to exhibit deformation pattern like Ti64, it indicated good metallurgical bonding of the interlayer with the base material. This resulted into the improved interfacial shear strength, 419 MPa, about 57% of Ti64 and 114% of SS410, as observed in Fig. 8b. Such enhanced interfacial shear strength is due to the improved diffusion of Ti and V into Nb region, as seen in the elemental dot maps in Fig. 4. It was hypothesized that bimetallic joints produced via LENS are more likely to be stronger in comparison to other joining techniques. This was evident in our case compared to the maximum shear strength, 217 MPa, reported by Kundu et al. [29] during diffusion bonding of CPTi and SS304 with Nb interlayer. This value was about 73% and 38% of the base materials, respectively. In another instance, Zakipour et al. [17] recorded a maximum interfacial shear strength of 220 MPa during bonding of stainless steel (316L) to Ti64 with Cu interlayer using transient liquid phase processing method.

From Fig. 9b, the fractography of the sheared bimetallic-joint sample showed cleavage and intergranular fracture, which resembles brittle failure, in agreement with the shear deformation behavior. Similar failure pattern was reported elsewhere [17, 29]. Although the morphologies of the fractured surfaces of Ti64 and SS410 samples were characterized with cleavage/flat-islands and coarsen dimples, Fig. 9a and c, which described brittle and ductile failures, respectively; the bimetallic joint's fractography was not a combination of those failure patterns. This was not surprising due to the presence of an interlayer. While Nb-interlayer serves as a diffusion barrier for the base-metals, it provided a pathway to improve

interfacial bond strength via upward-diffusion mechanism. This was evident in this experiment as Ti and V diffused into Nb bond region, while Nb itself diffused into SS410, Figs. 3 and 4, avoiding diffusion of Fe into Ti and formation of undesirable Fe-Ti brittle intermetallic phases.

Besides shear test, analysis of the bimetallic-joint's interfacial failure behavior during uniaxial loading could provide additional performance measure for the mechanical reliability of the structure. During compression test of the bimetallic joint, soft-section deformed more than the hard-section. But, we focused on the average yield strength of the bimetallic structure alongside the fracture pattern at the bond layer. From the stress-strain curves of the samples obtained after compression test, Fig. 10a, Ti64 sample exhibited a distinct elastic zone and yield point like the deformation behavior observed in shear test. Likewise, SS410 sample showed small elastic region with a large plastic zone, a deformation behavior that characterized ductile material similar to shear test. Bimetallic joint, on the other hand, showed deformation behavior that transitioned smoothly from elastic to plastic zone without a clear point of change in contrast to shear test. The reason for such variation is that compressive deformation in bimetallic structure is a cumulative effect within the bulk of the structure, comprising the base materials and the interfacial zone. Based on the direction of loading on our bimetallic-joint sample during the test, deformation transitioned from the soft material (SS410) to the hard material (Ti64) via the Nb interlayer. This deformation pathway potentially influenced the stress-strain curve, unlike shear deformation, which was primarily on the bimetallic interface, a small section of the overall structure. From Fig. 10b, the bimetallic sample exhibited a 0.2% compressive yield strength (YS) of 560 ± 4 MPa, about 46% and 169% of the LENS processed Ti64 and SS410 samples, respectively. Again, the bimetallic structure processed via LENS showed a considerable increase in compressive YS compared to maximum tensile strength obtained from diffusion bonded CPTi/stainless steel joints [13, 29, 30]. After compression deformation, crack growth at the SS410/Nb interface seemed to be arrested at the Nb region, Fig. 11. This indicated high resistance to failure at the region resulting from the formation of NbC phase.

5. Conclusion

A Ti64/SS410 bimetallic joint with Nb interlayer was developed using laser engineered net shaping (LENS) process. SEM images revealed interfacial microstructures with no cracking or de-bonding, which suggested good metallurgical bonding and the compatibility of Nb to Ti64 and SS410 materials. EDS dot maps showed upward diffusion of Ti, V and Nb, elements, while XRD analysis identified peaks of FeNb and β-Ti+Nb phases among others. No brittle intermetallic phases like FeTi and Fe_2Ti were found. This indicated that Nb acted not only as an intermediate bond layer (IBL), but also as diffusion barrier layer, mitigating the formation of brittle intermetallic phases, including lowering induced thermal stresses responsible for bimetallic- joint's interfacial cracking and low bond strength. From the mechanical reliability test, the interfacial shear strength as well as the overall compressive yield strength of the bimetallic structure processed via LENS were 419± 3 MPa and 560 ± 4 MPa, respectively. These values were about 14% and 69% more than SS410. The increase in shear and compressive yield strengths over the base material indicated improved interfacial bonding. Also, the interfacial region exhibited good resistance to crack propagation as was

observed on the backscattered electron image. In general, use of suitable IBL with appropriate joining process proved to be a good strategy to develop a mechanically reliable bimetallic joint of immiscible dissimilar metals. A proof-of concept part for direct application of the bimetallic-joint was demonstrated by welding base metals to its ends to form a reliable structural assembly. The development of such advanced composite-material-joint will, among other benefits, can enhance the weldability of dissimilar materials, which were previously difficult by direct joining through conventional methods.

Acknowledgements

Authors would like to acknowledge financial support from the National Science Foundation under the grant number NSF-CMMI 1538851 (PI - Bandyopadhyay) and the National Institute of Arthritis and Musculoskeletal and Skin Diseases of the National Institutes of Health under Award Number R01 AR067306-01A1. The content is solely the responsibility of the authors and does not necessarily represent the official views of the National Institutes of Health.

References

1. Onuike B, Heer B, Bandyopadhyay A Additive manufacturing of Inconel 718 – Copper alloy bimetallic structure using laser engineered net shaping (LENS™), Additive Manufacturing 21 (2018) 133–140.
2. Bandyopadhyay A, Heer B, Additive manufacturing of multi-material structures, Mater. Sci. Eng. R Rep 129 (2018) 1–16.
3. Peters M, Kumpfert J, Ward CH, Leyens C, Titanium alloys for aerospace applications, Adv. Eng. Mater 5 (2003) 419–427.
4. Niinomi M, Mechanical biocompatibilities of titanium alloys for biomedical applications, Journal of the Mech. Behavior of Biomedical Matl. (2008) 30–42.
5. Bandyopadhyay A, Krishna BV, Xue W, Bose S, Application of Laser Engineered Net Shaping (LENS) to manufacture porous and functionally graded structures for load bearing implants, J. Mater. Sci. Mater. Med 20 (2008) 29.
6. Sandmeyer Steel Company, Specification Sheet: Alloy 410, https://www.sandmeyersteel.com/images/410-Spec-Sheet.pdf, Accessed 2/11/2019.
7. Arafin MA, Medraj M, Turner DP, Bocher P, Effect of alloying elements on the isothermal solidification during TLP bonding of SS 410 and SS 321 using a BNi-2 interlayer, Materials Chemistry and Physics 106 (2007) 109–119.
8. Chen S, Zhang M, Huang J, Cui C, Zhang H, Zhao X, Microstructures and mechanical property of laser butt welding of titanium alloy to stainless steel, Materials and Design 53 (2014) 504–511.
9. Chen H-C, Bi G, Lee BY, Cheng CK, Laser welding of CPTi to stainless steel with different temporal pulse shapes, Journal of Matls. Processing Technology 231 (2016) 58–65.
10. Akbari Mousavi SAA, Farhadi Sartangi P Experimental investigation of explosive welding of CP-titanium/AISI 304 stainless steel. Materials and Design 30 (2009) 459–468.
11. Fazel-Najafabadi M, Kashani-Bozorg SF, Zarei-Hanzaki A, Dissimilar lap joining of 304 stainless steel to CP-Ti employing friction stir welding, Materials and Design 32 (2011) 1824–1832.
12. Campo KN, Campanelli LC, Bergmann L, dos Santos JF, Bolfarini C, Microstructure and interface characterization of dissimilar friction stir welded lap joints between Ti–6Al–4V and AISI 304, Materials and Design 56 (2014) 139–145.
13. Zakipour S, Halvaee A, Amadeh AA, Samavatian M, Khodabandeh A, An investigation on microstructure evolution and mechanical properties during transient liquid phase bonding of stainless steel 316L to Ti–6Al–4V, J. of Alloys and Compounds 626 (2015) 269–276.
14. Norouzi E, Atapour M, Shamanian M, Allafchian A, Effect of bonding temperature on the microstructure and mechanical properties of Ti-6Al-4V to AISI 304 transient liquid phase bonded joint, Materials and Design 99 (2016) 543–551.

15. Vigraman T, Ravindran D, Narayanasamy R, Effect of phase transformation and intermetallic compounds on the microstructure and tensile strength properties of diffusion-bonded joints between Ti–6Al–4V and AISI 304L, Materials and Design 36 (2012) 714–727
16. Kundu S, Sam S, Chatterjee S, Interface microstructure and strength properties of Ti–6Al–4V and microduplex stainless steel diffusion bonded joints, Materials and Design 32 (2011) 2997–3003.
17. Qin B, Sheng G M, Huang J W, Zhou B, Qiu S Y, Li C. Phase transformation diffusion bonding of titanium alloy with stainless steel. Mater Charact. 2006;56(1):32–8.
18. Ghosh M, Chatterjee S. Effect of interface microstructure on the bond strength of the diffusion welded joints between titanium and stainless steel. Mater Charact 2005;54(4):327–37.
19. Reichardt A, Dillonb RP, Borgonia JP, Shapiro AA, McEnerney BW, Momose T, Hosemann P, Development and characterization of Ti-6Al-4V to 304L stainless steel gradient components fabricated with laser deposition additive manufacturing, Materials and Design 104 (2016) 404–413.
20. Sahasrabudhe H, Harrison R, Carpenter C, Bandyopadhyay A, Stainless steel to titanium bimetallic structure using LENSTM, Additive Manufacturing 5 (2015) 1–8.
21. Iron-Titanium (Fe-Ti) Binary Phase Diagram, Alloy Phase Diagrams, ASM Handbook vol. 3, Murray JL 1992.
22. Onuike B, Bandyopadhyay A, Additive manufacturing of Inconel 718 – Ti6Al4V bimetallic structures, Additive Manufacturing 22 (2018) 844–851
23. Kundu S, Chatterjee S, Olson D, Mishra B, Effects of intermetallic phases on the bond strength of diffusion-bonded joints between titanium and 304 stainless steel using nickel interlayer. Metall. Mater Trans A 2007;38(9):2053–60.
24. Kundu S, S Chatterjee. Interfacial microstructure and mechanical properties of diffusion-bonded titanium–stainless steel joints using a nickel interlayer. Mater Sci Eng A 2006;425(1):107–13
25. Kundu S, Ghosh M, Laik A, Bhanumurthy K, Kale GB, Chatterjee S, Diffusion bonding of commercially pure titanium to 304 stainless steel using copper interlayer. Mater Sci Eng A2005;407(1):154–60.
26. Tomashchuk I, Sallamand P, Belyavina N, Pilloz M,, Evolution of microstructures and mechanical properties during dissimilar electron beam welding of titanium alloy to stainless steel via copper interlayer, MaterialsScience&EngineeringA585(2013)114–122.
27. Elrefaey A, Tillman W, Solid state diffusion bonding of titanium to steel using a copper base alloy as interlayer. J Mater Process Technol 209 (2009) 2746–52.
28. Balasubramanian M, Characterization of diffusion-bonded titanium alloy and 304 stainless steel with Ag as an interlayer, Int J Adv Manuf Technol. 82 (2016) 153–162
29. Kundu S and Chatterjee S, Evolution of Interface Microstructure and Mechanical Properties of Titanium/304 Stainless Steel Diffusion Bonded Joint Using Nb Interlayer, ISIJ International, vol. 50 (2010), No. 10, pp. 1460–1465
30. Lee JG, Hong SJ, Lee MK, Rhee CK, High strength bonding of titanium to stainless steel using an Ag interlayer. J. Nucl Mater 2009;395(1):145–9.
31. Shiue RK, Wu SK, Infrared brazing of Ti–6Al–4V and 17–4 PH stainless steel with (Ni)/Cr barrier layer(s). Mater Sci Eng A 2008;488(1):186–94.
32. Li P, Li J, Xiong J, Zhang F, Raza SH, Diffusion bonding titanium to stainless steel using Nb/Cu/Ni multi-interlayer. Mater Charact. 68 (2012) 82–7.
33. Bandyopadhyay A, Bose S, Additive Manufacturing, Published by CRC Press Taylor & Francis Group, FL. US, 2015.
34. Onuike B, Bandyopadhyay A, Bond strength measurement for additively manufactured Inconel 718-GRCop84 copper alloy bimetallic joints, Additive Manufacturing 27 (2019) 576–585. [PubMed: 31372350]
35. ASM Aerospace Specification Metals Inc., Titanium Ti-6Al-4V (Grade 5), Annealed, ASM Material Data Sheet, http://asm.matweb.com/search/SpecificMaterial.asp?bassnum=mtp641 Accessed, 2/13/19.
36. Murr LE, et al., Microstructure and mechanical behavior of Ti–6Al–4V produced by rapid-layer manufacturing, for biomedical applications, Journal of the Mechanical Behavior of Biomedical Materials 2 (2009) 20–32 [PubMed: 19627804]

37. Hamilton Precision Metals, SS410 Technical Data Sheet, https://www.hpmetals.com/-/media/ametekhpmetals/files/technical-data/stainless-steel/ss%20410.pdf Accessed 2/13/19

Highlights

- Processing of Ti6Al4V and SS410 as a bimetallic joint using laser-based directed energy deposition (DED) system.
- Niobium (Nb) was used as a bond layer between the twimmiscible base-materials.
- The bimetallic joint showed improved bond strength, both under compression and shear loading.
- Proof-of-concept part for direct application of the bimetallic joint was demonstrated by welding base metals, end-to-end, tthe joint.

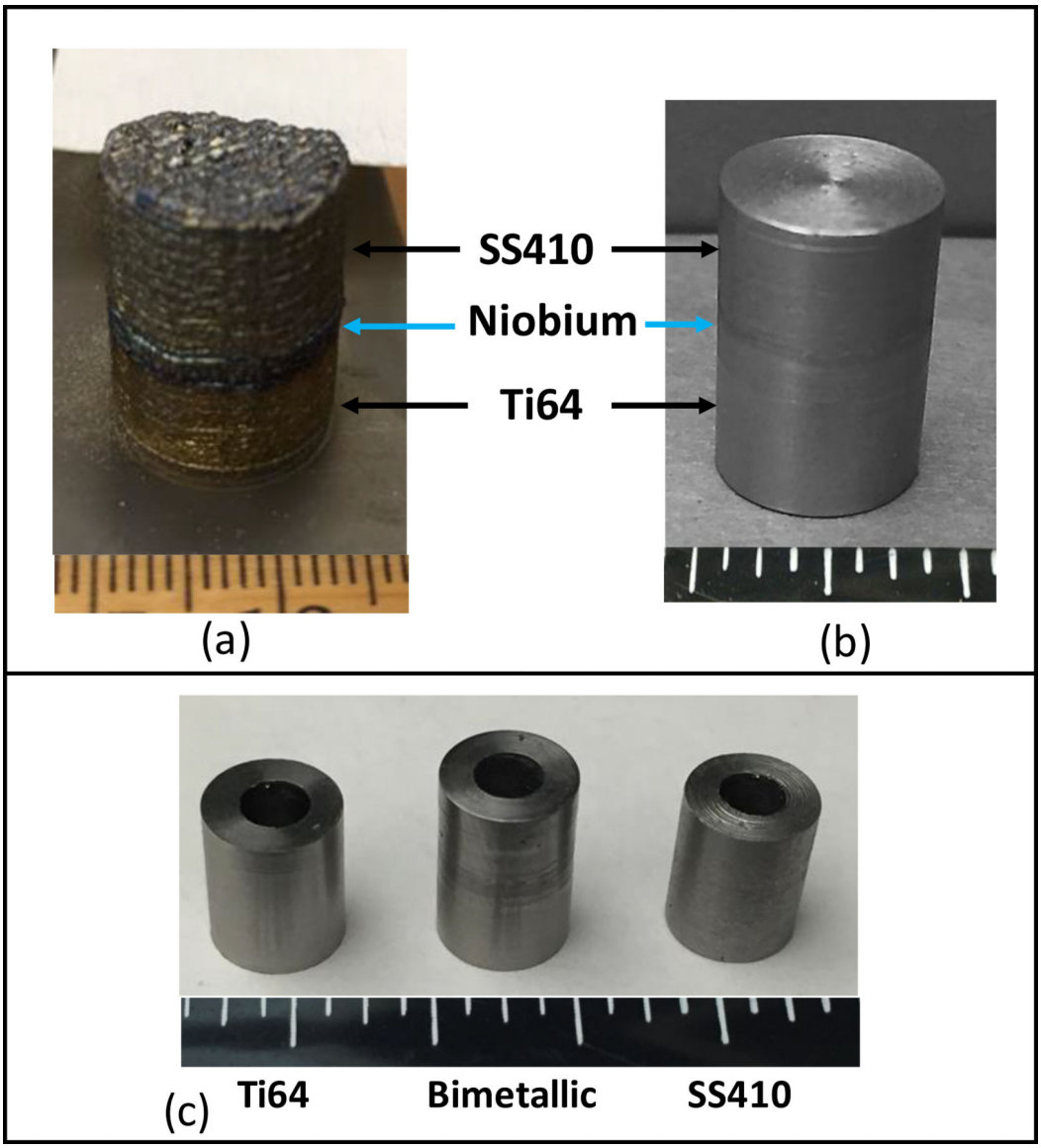

Fig. 1.

Ti64/SS410 bimetallic joint with Niobium interlayer. (a) As-printed, (b) After machining and (c) Tubes of the base materials and the bimetallic joint.

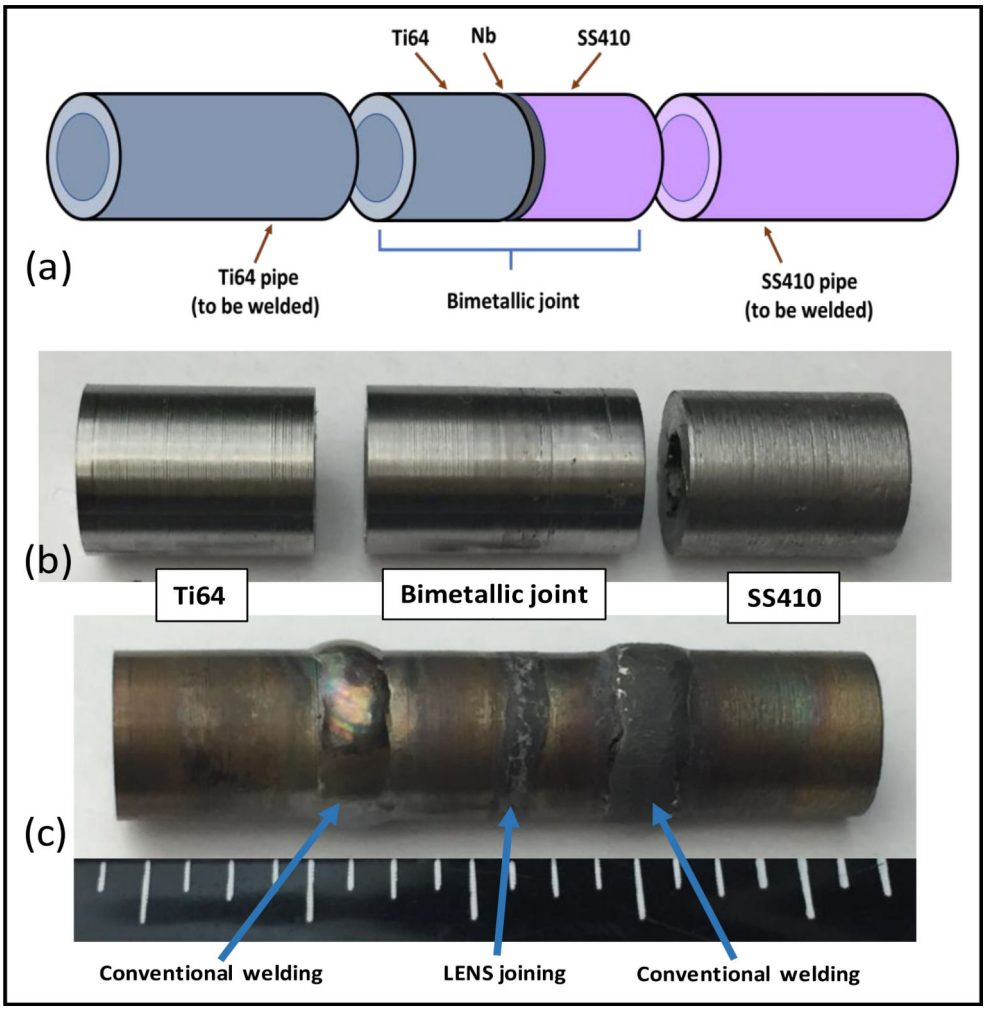

Fig. 2.

Bimetallic joint application. (a) Concept model for joining dissimilar materials, (b) Un-welded parts to bimetallic joint and (c) Welded assembly.

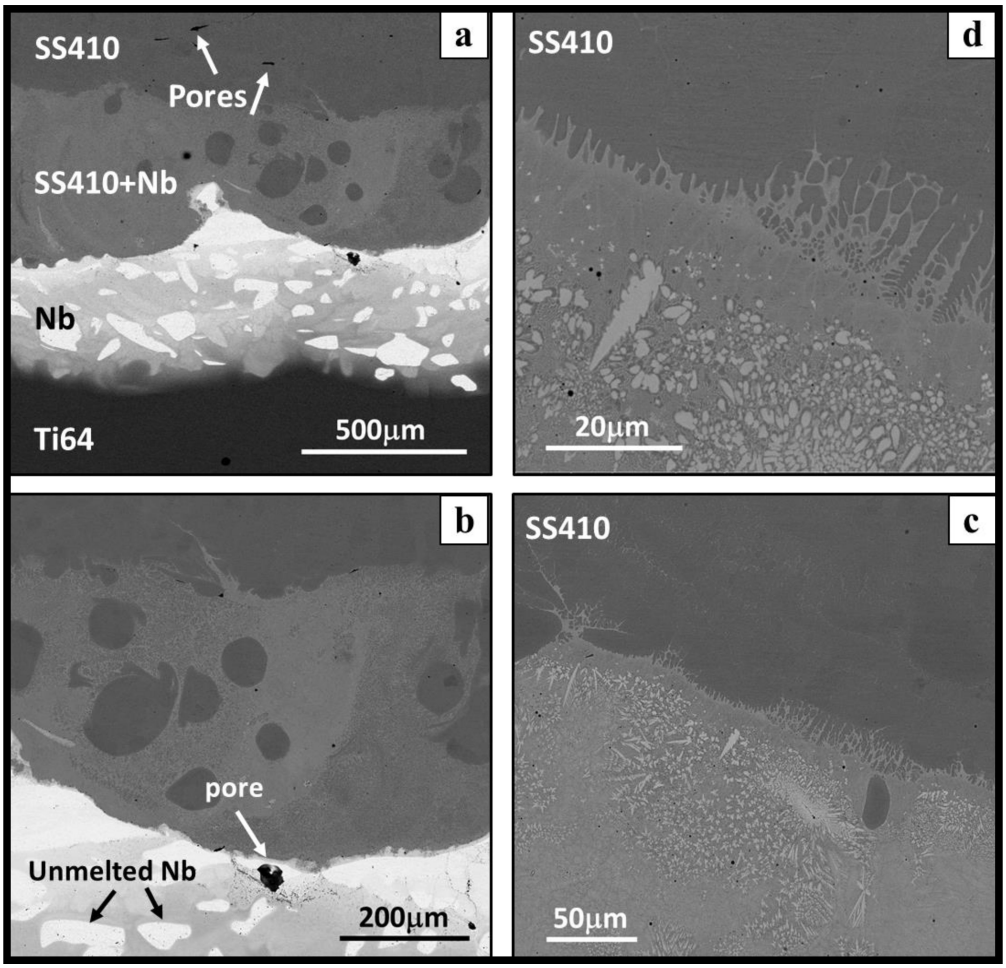

Fig. 3.
BSE images of the bimetallic interfacial features/microstructures.

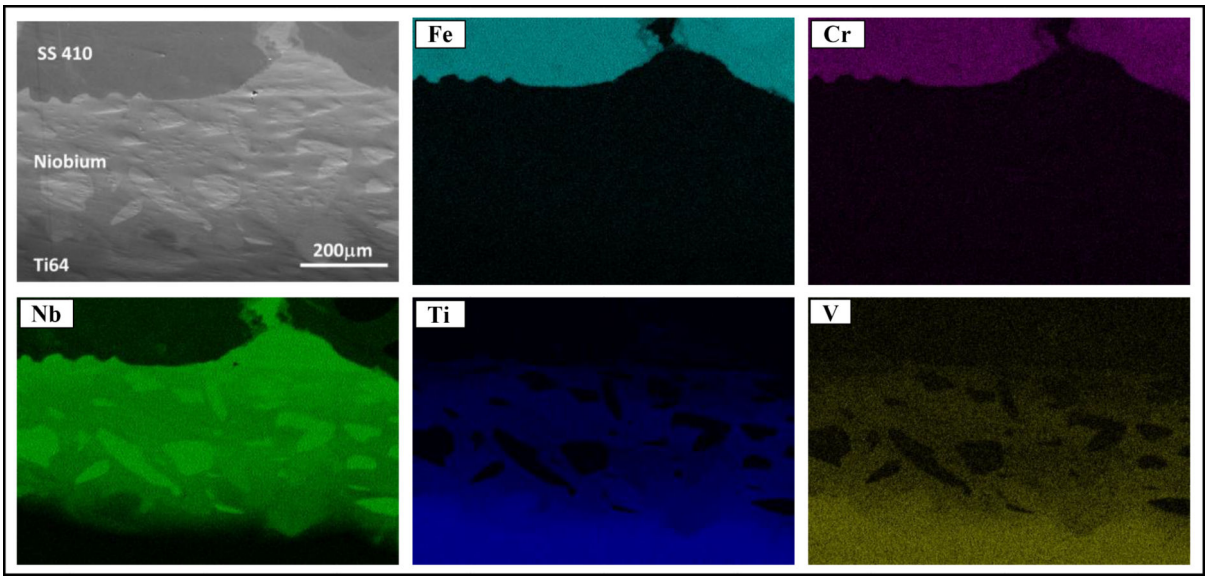

Fig. 4a.

EDS dot map of the bimetallic joint's interface showing upwards diffusion of Ti and V elements into Nb, including elemental diffusion of Nb into SS410 region.

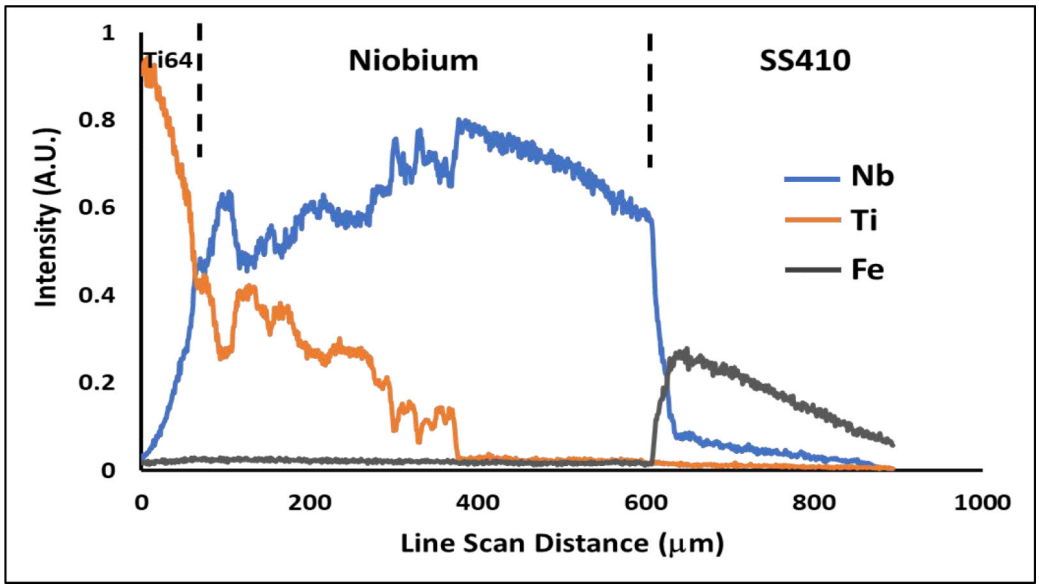

Fig. 4b.

EDS line-scan of the bimetallic joint's interface showing diffusion of Ti into Nb, including elemental diffusion of Nb into SS410 region.

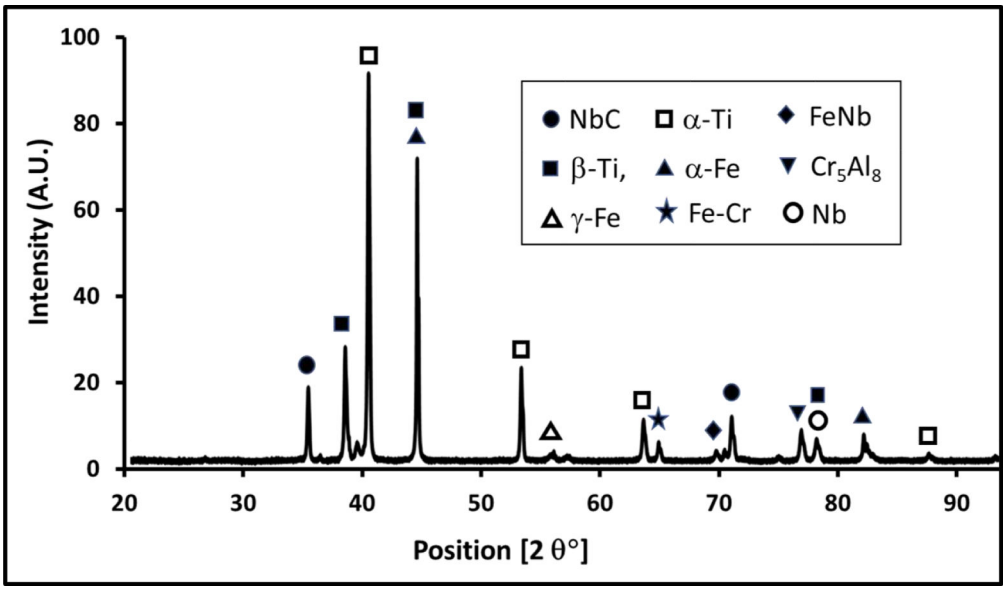

Fig. 5.
X-ray diffraction analysis of the bimetallic cross-section.

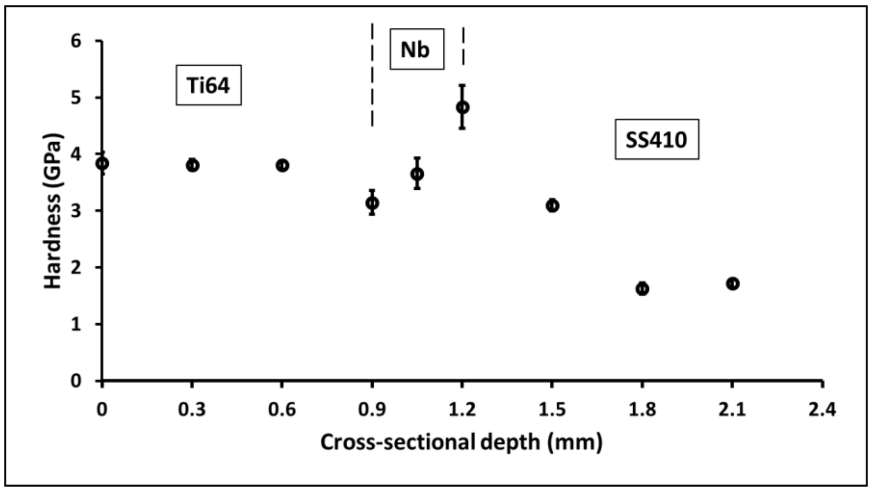

Fig. 6.
Bimetallic-joint interfacial hardness profile.

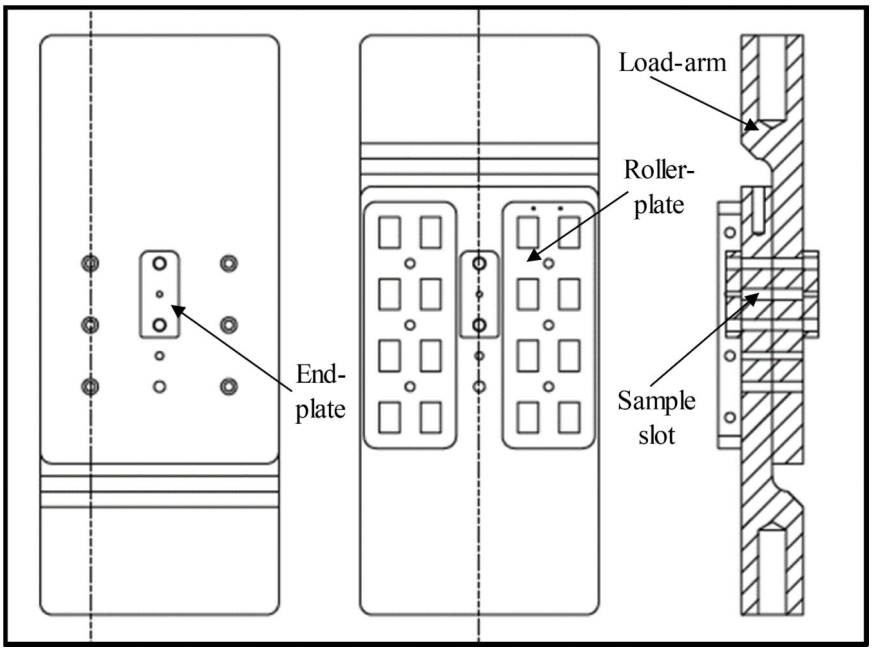

Fig. 7.
Schematic of the single-shear test device.

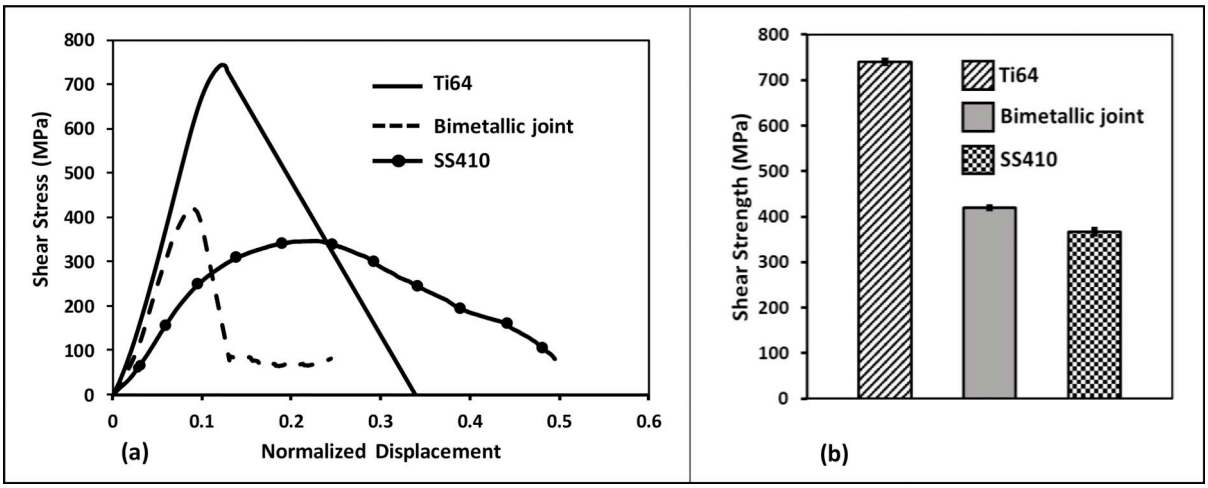

Fig. 8.

Shear properties: (a) Shear stress vs. normalized displacement curves, (b) Shear strengths for LENS processed Ti64, SS410 and the bimetallic joint samples.

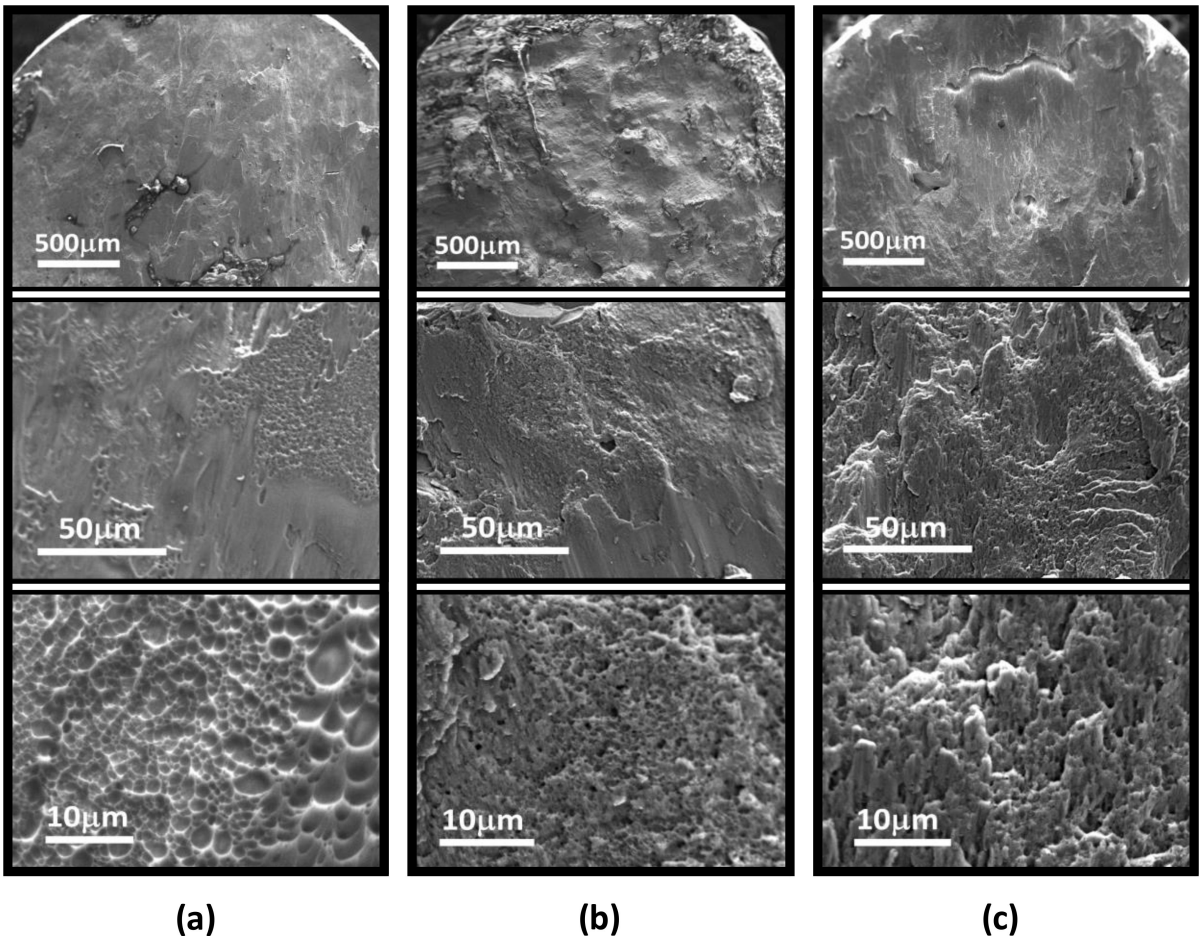

Fig. 9.
SEM images of sheared surfaces. (a) Ti64, (b) Bimetallic joint and (c) SS410 samples.

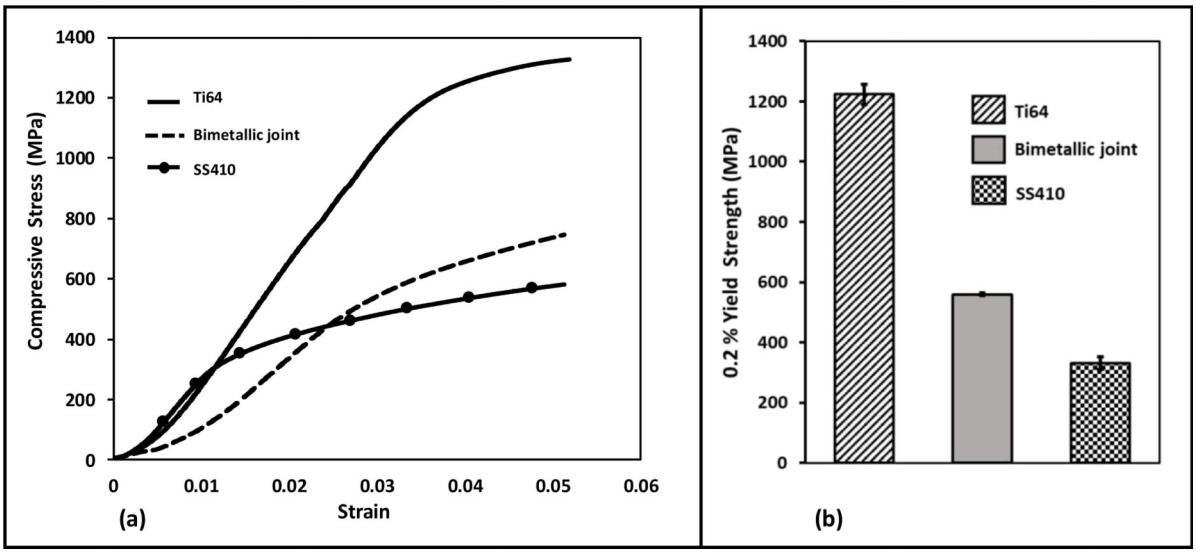

Fig. 10.

Compressive strength properties: (a) Compressive stress - strain curves, (b) 0.2 % Yield strengths of the LENS processed Ti64, SS410 and the Bimetallic joint samples.

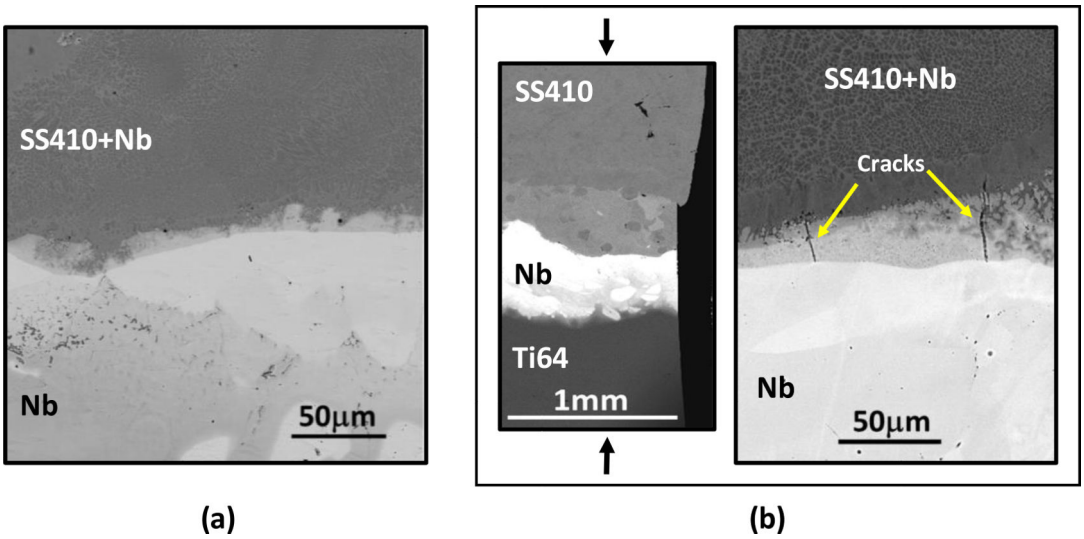

Fig. 11.

Backscattered electron images of the bimetallic joint cross-section for compression test. (a) Before testing and (b) after testing.

Table 1.

LENS process parameters for Ti64-SS410 Bimetallic joint with Nb interlayer

Material	Laser power (W)	Laser scan hatch speed (m/min)	Laser scan contour speed (m/min)	Hatch distance (μm)	Layer thickness (μm)
Ti64	375	0.4	0.3	530	200
Nb	450	0.4	0.3	530	150
SS410	375	0.4	0.3	530	200

Powder feed rate ~12 (g/min)

Table 2:

Mechanical properties results

Material	Shear strength (MPa)	0.2% Yield Strength (MPa)
Ti64	7 0 ± 5	1224 ± 34
Bimetallic joint	419 ± 3	560 ± 4
SS410	367 ± 6	331 ± 21